Proceedings of the 17th World Congress
The International Federation of Automatic Control
Seoul, Korea, July 6-11, 2008

Novel Causal Digraph Reasoning For Fault Diagnosis with Application on the Paper Machine Short Circulation Process

Hui Cheng, Mats Nikus, Sirkka-Liisa Jämsä-Jounela

Laboratory of Process Control and Automation
Helsinki University of Technology
Kemistintie 1, FI-02150 HUT, Finland, (chenghui@cc.hut.fi)

Abstract: This paper presents an enhanced dynamic causal digraph reasoning method for fault diagnosis and its application to the short circulation process of a paper machine. In order to improve the isolation capability of the original method, an inference mechanism between the arcs of the graph is proposed to locate process faults on the arcs. Application of the proposed method to the paper machine short circulation process is presented at the end of the paper. The results show that the proposed method is able to identify the responsible arcs when the system is affected by a process fault.

1. INTRODUCTION

Research in the field of fault diagnosis has been very active since the 70s. In order to meet the demands from industry concerning quality, efficiency and safety, numerous fault diagnosis methods have been developed. Of these, causal model based method has attracted remarkable attention since it was first developed by Iri et al. (1979). As a modelling method, the causal model is able to describe the system behaviour with cause-effect relationships between the entities of a system (Fagarasan et al., 2004). The causal models can be used for different purposes, such as simulation (Leyval et al., 1994) and fault diagnosis (Montmain et al., 2000).

Since Iri et al. (1979) introduced the Signed Directed Graph (SDG), the simplest causal digraph method, into the field of fault diagnosis, it has made remarkable progress. In order to alleviate the problem with spurious results, fuzzy logic was used by Shih (1995) to represent both the variables and the relationships. Another improvement of the causal digraph was the introduction of the piece-wise linear transfer functions (QTF) by Leyval et al. (1994). Recently more quantitative models, such as difference-algebraic equations (Montmain et al., 2000) have been used in causal digraph for further improvement.

As reported by Montmain (2000) and Fagarasan (2004), the dynamic causal digraph method is able to manage different types of fault: sensor, actuator and process faults. However, the ability of the dynamic causal digraph method to handle process faults is limited. The method assumes that a primary fault is a change in a variable (a node in the digraph) rather than a change in the consistency between the variables (an arc in the digraph). In industrial applications, however, it is usually required to know the corresponding faulty process components. Faulty nodes alone cannot provide enough information to identify the faulty process components. One important topic is therefore to locate the responsible arcs, and an inference mechanism between arcs has been developed by the authors to achieve this aim.

The paper is organized as follows. In Section 2 the enhanced dynamic causal reasoning method is proposed. In Section 3 the testing environment is introduced. The fault diagnosis results of two fault scenarios are given in Section 4. The conclusions are drawn in Section 5.

2. ENHANCED DYNAMIC CAUSAL DIGRAPH

An enhanced dynamic causal digraph method designed to locate the process fault on the arcs is proposed in this Section. The proposed method performs the fault detection and isolation in four steps as follows

1. Generate the global (*GR*) and local residuals (*LR*)
2. Detect a possible abnormality in the residual signals using the CUSUM method
3. For the variables in the detection set, locate the primary fault and identify its nature by means of the fault isolation and nature rules
4. In case of a process fault, an additional inference step between arcs is performed in order to locate the fault on the responsible arc(s)

Discrete-time state space models are used to describe the cause-effect relationships in this paper.

2.1 Residual generation with the dynamic causal model

The dynamic causal digraph produces two kinds of residuals to be used in fault detection and isolation: global and local residual. The global residual is produced for fault detection by the difference between the measurement and the global propagated value as in

$$\begin{aligned} GR(Y) &= Y(k) - \hat{Y}(k) \\ \hat{X}(k+1) &= A\hat{X}(k) + B\hat{U}(k) \\ \hat{Y}(k) &= C\hat{X}(k) \end{aligned} \tag{1}$$

where *Y(k)* is the measurement and $\hat{Y}(k)$ is the global propagation value obtained from model in (1) with input as $\hat{U}(k) = \left[\hat{U}_1(k),...,\hat{U}_n(k)\right]^T$, the lagged global propagation value from the predecessors in the digraph, and *n* denotes the number of inputs for variable *Y*.

The local residuals are subcategorized into three types: individual local residuals (*ILR*), multiple local residuals (*MLR*) and total local residuals (*TLR*). The *ILR* is produced by taking the difference between the measurement and the local propagation value which is obtained from the same model in (1) with the input vector as $U(m,k) = \left[\hat{U}_1(k),..U_m(k),..\hat{U}_n(k)\right]^T$, where $U_m(k)$ is the measurement for the parent node. Similarly, the $MLR_Y(P)$ is produced with input $U(P,k) = \left[\hat{U}_1(k),..,U_j(k),...,\hat{U}_n(k)\right]^T$, $j \in P$, P is the set of subscripts of the predecessors which use the measurement as an input. The $TLR(Y)$ is produced with $P = P_Y$, where P_Y is the set of subscripts of all the predecessors of *Y*.

2.2 Residual evaluation with the CUSUM method

The CUSUM method is used to evaluate the generated residual signals with respect to its insensitivity to the noise and outliers in the measurements. Moreover, the CUSUM method is able to detect both positive and negative jumps in the mean of the residual signal. In the fault free case, the residuals are assumed to be zero mean random signals, and in the case of a fault the mean value of the residual signal is changing in either a positive or a negative direction.

The CUSUM algorithm (Mogens et al., 2003) for positive mean changes is given by the following equations:

$$S(k) = S(k-1) + \frac{\mu_1 - \mu_0}{\sigma^2}\left(r(k) - \frac{\mu_0}{2} - \frac{\mu_1}{2}\right) \qquad (2)$$
$$m(k) = \min\left(m(k-1), S(k)\right)$$

where *S(k)* is the cumulative sum at time instant *k*, μ_1 is a user specified minimum detectable change, $r(k)$ is the residual signal, μ_0 is the mean value of the nominal signal and σ is the standard deviation of the fault free residual. Whenever $S(k) - m(k) > \lambda$, a change is detected. λ provides robustness to the fault detection however delays the detection too. The algorithm for the detection of negative mean jumps can be obtained by modifying (2). In the rest of the paper, the result of the CUSUM calculation will be denoted as a function: $CU(\,)$.

2.3 Fault isolation reasoning with rules

Fault isolation is performed recursively for the nodes in the detection set by using a set of rules developed by Montmain and Gentil (2000), which are converted into a table as shown in Table 1. After fault isolation, the nature of the fault is identified by testing how the faults propagate to their children nodes. If the fault propagates through the digraph globally, it is identified as a process fault; otherwise it is defined as a local measurement fault. The respective rules are given in Table 2.

Table 1. Fault isolation rules of the dynamic causal digraph

$CU(GR(Y))$	$CU(TLR(Y))$	$CU(ILR_Y(m))$	$CU(ILR_Y(i))$	$CU(MLRY(P_1))$	$CU(MLR_Y(P_2))$	Decision
0	0	0	0	0	0	No fault
1/−1	0	0*	1/−1*	0*	1/−1*	Fault propagates from the parent node *m*
1/−1	0	1/−1**	1/−1**	1/−1**	0**	Fault propagates from the nodes with subscript in P_2
1/−1	1/−1	1/−1	1/−1	1/−1	1/−1	Local fault on variable *Y*

* $\forall i \neq m, i \in P_Y$, $m \in P_1$, $m \notin P_2$, P_Y is the set of subscripts of parents nodes of the node *Y*.

** $\forall i, m, i \in P_Y, m \in P_Y$, $\forall P_1, P_2 \subseteq P_Y$

Table 2. Fault nature rules of the dynamic causal digraph

$CU(GR(X))$*	$CU(TLR(X))$	Fault nature
1/−1	1/−1	Local fault for that child node
1/−1	0	Process fault for the faulty node
0	1/−1	Sensor fault for the faulty node

**X* is the subscript of any child nodes of the node *Y*.

2.4 Locating the process fault on the arcs

In the case of a process fault, locating it on the arcs is also desirable. However, the MISO structure of the digraph causes problems by generating spurious results, which are the non-unique explanations to the fault. In order to decrease the number of spurious results, a new inference mechanism between the arcs is proposed for evaluating the sets of suspected arcs. The idea behind is to test the consistency between the sets of suspected arcs formed from fault origins and the knowledge of the output arcs from the same node.

The knowledge matrix of the whole digraph is formed by the knowledge matrices of each node which has output arcs. The matrix $\mathbf{M}_U$ for a node, U, is formed as in

$$\mathbf{M}_U(i,j)=\begin{cases}1, \text{faulty arc} < U, i > \text{causes the fault of} < U, j > \\ 0, \text{otherwise}\end{cases} \quad (3)$$

The dimension of the matrix $\mathbf{M}_U$ is $n \times n$, if n is the number of output arcs that node U has. The knowledge matrix $\mathbf{M}$ for digraph is obtained by merging the knowledge matrices of individual nodes as $\mathbf{M}=\text{blockdiag}(\mathbf{M}_1, \mathbf{M}_2, .., \mathbf{M}_l)$, where l denotes the number of nodes that have output arcs in the digraph. $\mathbf{M}$ has the dimension $N_a \times N_a$, where N_a is the number of arcs in the digraph, and each row or column represents one arc in the digraph.

The consistency test between the sets of suspected arcs and the knowledge matrix $\mathbf{M}$ is performed by matrix manipulation. First, one row vector **sv** with length N_a is formed for one specific set of suspected arcs S as in

$$\mathbf{sv}(i)=\begin{cases}1, \text{if } \ ARC(\mathbf{M}, i) \in S, 1 \le i \le N_a \\ 0, \text{otherwise}\end{cases} \quad (4)$$

where $ARC(\mathbf{M}, i)$ gives the arc corresponding to the ith row in the matrix $\mathbf{M}$. The set S is considered as a possible result only when the number of nonzero entries in the obtained row vector does not change when compared to the row vector **sv**

$$NUM(\mathbf{sv}) = NUM(\mathbf{sv} \cdot \mathbf{M}) \quad (5)$$

where $NUM()$ gives the number of nonzero entries in the matrix.

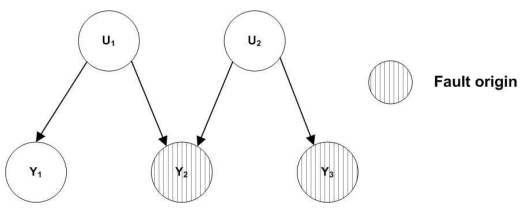

Fig. 1. Example of inference between arcs.

Figure 1 illustrates the operation of the proposed inference mechanism between arcs. The assumption is made that the nodes Y_2 and Y_3 are identified as fault origins for the process fault. The knowledge between arcs is first introduced into the digraph. For the node U_1, if the fault on the arc $<U_1, Y_2>$ always causes the fault on the arc $<U_1, Y_1>$, while not vice verse, the matrix $\mathbf{M}_{U_1}$ can be formed as in

$$\mathbf{M}_{U_1}=\begin{bmatrix}1 & 0\\ 1 & 1\end{bmatrix}, \mathbf{M}_{U_2}=\begin{bmatrix}1 & 1\\ 1 & 1\end{bmatrix} \Rightarrow$$

$$\mathbf{M}=\text{blockdiag}(\mathbf{M}_{U_1}, \mathbf{M}_{U_2})=\begin{bmatrix}1 & 0 & 0 & 0\\ 1 & 1 & 0 & 0\\ 0 & 0 & 1 & 1\\ 0 & 0 & 1 & 1\end{bmatrix} \quad (6)$$

Similarly the matrix $\mathbf{M}_{U2}$ is formed for the node U_2 and the knowledge matrix $\mathbf{M}$ of the digraph is obtained in (6). The corresponding arcs of each row of matrix $\mathbf{M}$ are $<U_1, Y_1>$, $<U_1, Y_2>$, $<U_2, Y_2>$ and $<U_2, Y_3>$. It can be seen from Figure 1 that there are three sets of suspected arcs, {$<U_1, Y_2>$, $<U_2, Y_2>$, $<U_2, Y_3>$}, {$<U_1, Y_2>$, $<U_2, Y_3>$} and {$<U_2, Y_2>$, $<U_2, Y_3>$}. For the first set, the **sv** vector is formed as [0 1 1 1] according to Equation 4, and the consistency check is

$$NUM(\mathbf{sv}) = 3 \neq NUM(\mathbf{sv} \cdot \mathbf{M}) = NUM(\begin{bmatrix}1 & 1 & 2 & 2\end{bmatrix}) = 4 \quad (7)$$

The result above implies that the first set of suspected arcs cannot be consistent with the knowledge matrix. For the same reason, the second set of arcs is excluded from the possible results. For the last set, **sv** vector is [0 0 1 1] and the consistency check is

$$NUM(\mathbf{sv}) = 2 = NUM(\mathbf{sv} \cdot \mathbf{M}) = NUM(\begin{bmatrix}0 & 0 & 2 & 2\end{bmatrix}) \quad (8)$$

The result indicates that the third set is the possible result. It can be seen that the proposed inference mechanism between arcs is able to decrease the number of sets of suspected arcs.

3. TESTING ENVIRONMENT

The proposed method was tested on the paper machine short circulation process, which was simulated using the Advanced Process Simulation Environment (APROS) developed by VTT (Technical Research Centre of Finland). A description of the short circulation process and the simulation environment are given in this Section.

3.1 Description of the short circulation process

The short circulation is a crucial part of the papermaking process, with several important functions. Firstly, the dilution of the fiber suspension entering the process to a suitable consistency for the headbox takes place in the short circulation. The short circulation also improves the economy

of the process by recycling the bypass fiber and filler. Last, the important paper quality controls, i.e. basis weight and ash rate are implemented here.

The short circulation process starts after a machine chest. Usually the machine chest is followed by a thick stock pump and a valve, which is used for basis weight control. The thick stock is pumped to the wire pit and mixed with white water and filler controlled by the filler valve. The diluted stock is pumped by a fan pump via the hydro-cyclones to the deculator and then pumped into the hydraulic headbox and sprayed onto the wire at a constant speed. On the wire the stock is dehydrated to form a wet web. About 98% of the water and 54% of the filler and fibre bypass the wire and flow to the wire pit as white water. The process is presented in Figure 2.

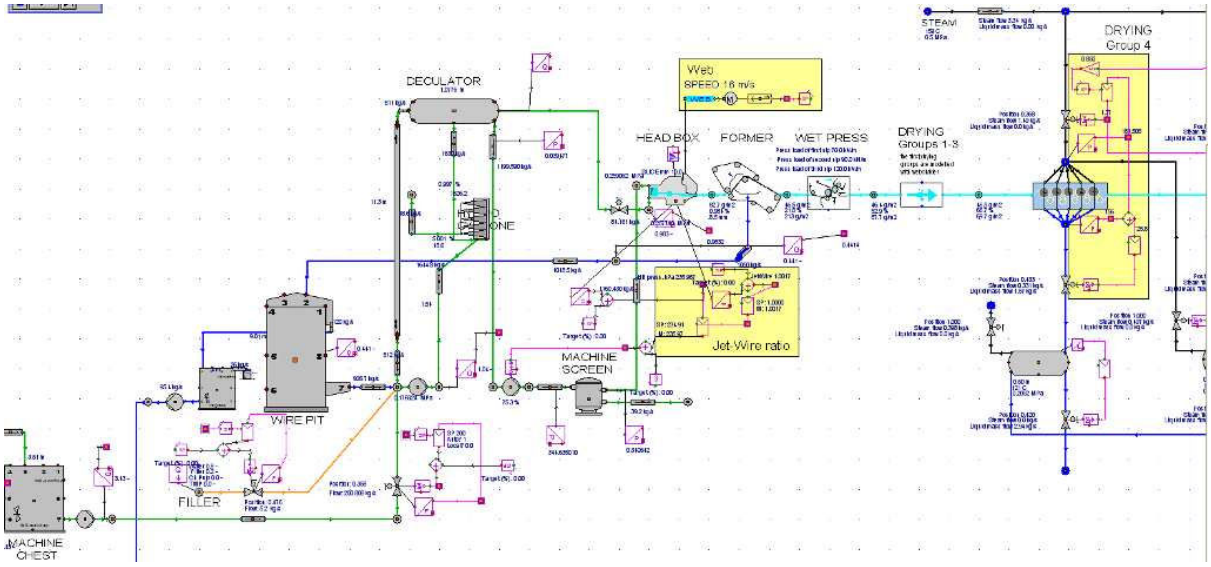

Fig. 2. Flowsheet of the short circulation and the APROS model for paper machine

The most important measurements in the short circulation process and the paper quality measurements are listed in Table 3.

Table 3. Description of important variables

Variables	Description	Unit
baval	Basis weight valve opening	-
wpfc	Filler consistency in the wire pit	%
wpfic	Fiber consistency in the wire pit	%
fival	Filler adding valve opening	-
defc	Filler consistency in the deculator	%
defic	Fiber consistency in the deculator	%
hbfic	Fiber consistency in the headbox	%
hbfc	Filler consistency in the headbox	%
feedpump	Headbox feed pump rotation	%
totalflow	Mass flow into the headbox	kg/s
bw	Basis weight of paper	g/m^2
ash	Ash consistency of paper	%

3.2 Simulation environment

The APROS paper machine simulator provides validated model algorithms for the process components mainly based on first principles. The simulation model is constructed by drawing the process flowsheet and setting up the parameters of the components (Lappalainen, 2003). One built-in paper machine model was provided by VTT. The control loops were added and the process components were parameterized according to a typical setup of the papermaking process. The APROS paper machine model is shown in Figure 2.

4. CASE STUDIES AND RESULTS

This paper provides two case studies concerning fault detection and isolation on the paper machine short circulation process. The two studied faults are: 1) fiber consistency in the deculator (sensor fault), and 2) filler retention drop on the wire section (process fault). The two fault scenarios, the experimental procedures and the results for each fault scenario are presented in the remainder of this Section.

4.1 Fault scenarios

Two different types of fault were introduced into the APROS paper machine model in sequence in order to test the proposed method. The first fault introduced was a sensor fault on the fiber consistency in the deculator. A drift fault with a slope of $3.5e^{-6}$%/s was added to the fault free measurement *defic*.

The second fault introduced was a process fault, in which the filler retention on the wire dropped. The filler retention rate is the measure of how much filler remain in the wet web after the wire section. The decrease of it will directly affect the ash rate of the final paper and result in the accumulation of the filler in the short circulation worsening the wear of equipment. The fault was simulated by changing the retention rate from 45% to 40%.

4.2 Description of the experiment

The case studies on the short circulation process were carried out in 3 steps. First the structure of the causal digraph model was decided, as shown in Figure 4.

Secondly, the simulation in an open loop was run for modelling the cause-effect relationships in the digraph, during which the basis weight valve, filler valve and feed pump for the headbox were adjusted manually. Nine discrete-time state space models for the causal digraph were identified.

The last step of the experiment was to run the simulation with the control loops closed. Two different artificial faults were introduced into the APROS model at the time intervals 1800–7800 s and 8800–17800 s respectively. The proposed method was then applied to detect and identify the faults. The total simulation time was 25800 seconds, and the sampling time was 10 seconds.

4.3 Diagnosis results for the first fault scenario

For the first fault scenario, the *GR*s shown in Figure 3 indicate that, during this time period (1800–7800 s), only the variable *defic* produced an alarm. The fault isolation rules clearly infer that the fault is local, and the nature rules infer that it is a sensor fault. Finally, the fault propagation path is shown as the fault diagnosis result in Figure 4.

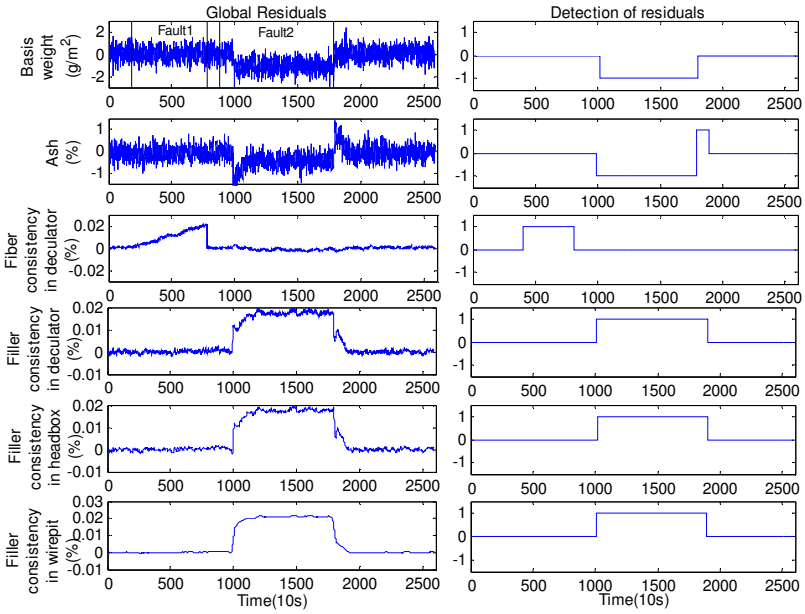

Fig. 3. Global residuals for the variables *bw*, *ash*, *defic*, *hbfic*, *defc*, and *wpfc*

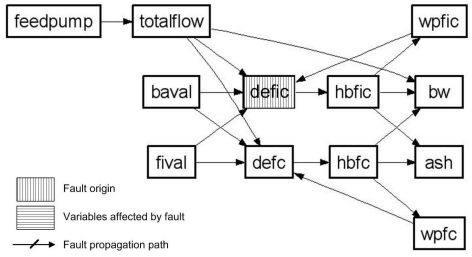

Fig.4. Diagnosis result of first fault

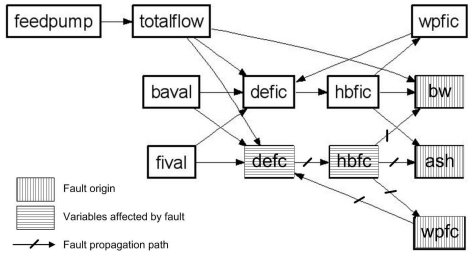

Fig.5 Diagnosis result of the second fault

4.4 Diagnosis results for the second fault scenario

During the second fault period, the variables *ash*, *bw*, *defc*, *wpfc* and *hbfc* were detected from the *GR*s shown in Figure 3, and the detection set was formed. *LR*s are generated for the variables in the detection set and fault isolation rules are applied. As the final fault diagnosis result, the fault propagation path is formed as shown in Figure 5, where all the variables in the detection set have been processed.

The fault was identified as a process fault by the fault nature rules because the fault propagated globally in the digraph. The responsible process component is then desired to find. However, spurious results were produced due to the multiple fault origins and multiple input arcs for each fault origin. In Figure 5 the fault origin nodes *wpfc*, *bw* and *ash* have five input arcs. Thus the $1\cdot(2^2-1)\cdot(2^3-1)=21$ exhaustive combinations of these arcs form the sets of suspected arcs such as: {<*hbfc*, *wpfc*>, <*totalflow*, *bw*>, < *hbfc*, *ash*>}, {<*hbfc*, *wpfc*>, <*hbfic*, *bw*>, <*hbfic*, *ash*>}…

In order to perform the inference between arcs, knowledge between arcs was introduced into the digraph model. The knowledge matrix $\mathbf{M}$ for the digraph is formed by the knowledge matrix of each node that has output arcs as in

$$\mathbf{M}_{feedpump}=1;\ \mathbf{M}_{totalflow}=\begin{bmatrix}1&0&0\\0&1&1\\0&1&1\end{bmatrix};\ \mathbf{M}_{baval}=\begin{bmatrix}1&0\\1&1\end{bmatrix};$$

$$\mathbf{M}_{fival}=\begin{bmatrix}1&1\\0&1\end{bmatrix};\ \mathbf{M}_{defic}=1;\ \mathbf{M}_{defc}=1; \tag{9}$$

$$\mathbf{M}_{hbfic}=\begin{bmatrix}1&1&1\\1&1&1\\1&1&1\end{bmatrix};\ \mathbf{M}_{hbfc}=\begin{bmatrix}1&1&1\\1&1&1\\1&1&1\end{bmatrix};\ \mathbf{M}_{wpfic}=1;$$

$$\mathbf{M}_{wpfc}=1;\ \mathbf{M}=\text{blockdiag}\begin{pmatrix}\mathbf{M}_{feedpump},\mathbf{M}_{totalflow},\mathbf{M}_{baval},\\\mathbf{M}_{fival},\mathbf{M}_{defic},\mathbf{M}_{defc},\\\mathbf{M}_{hbfic},\mathbf{M}_{hbfc},\mathbf{M}_{wpfic},\mathbf{M}_{wpfc}\end{pmatrix}$$

The knowledge included in the matrix **M** is based on process knowledge from paper machines. The sub matrix $\mathbf{M}_{hbfc} = \begin{bmatrix} 1 & 1 & 1 \\ 1 & 1 & 1 \\ 1 & 1 & 1 \end{bmatrix}$ represents the relationship between arc <*hbfc*, *bw*>, <*hbfc*, *ash*> and <*hbfc*, *wpfc*>. This sub matrix is obtained from the knowledge of the filler material balance. Whenever the filler flows to the wire pit decrease or increase, the filler flows to final production (*ash* and *bw*) increase or decrease. The same matrix $\mathbf{M}_{hbfic}$ is obtained for the arcs <*hbfic*, *bw*>, <*hbfic*, *ash*> and <*hbfic*, *wpfc*>.

With **M** in (9), the 21 sets of suspected arcs were tested with (5). The set of suspected arcs {<*hbfc*, *wpfc*>, <*hbfic*, *ash*>, <*hbfic*, *bw*>} is considered as an example as in

$$\begin{aligned} &\mathbf{sv} = [0\,0\,0\,0\,0\,0\,0\,0\,0\,0\,0\,1\,1\,0\,0\,1\,0\,0] \\ &NUM(\mathbf{sv}) = 3 \neq NUM(\mathbf{sv} \cdot \mathbf{M}) = \\ &NUM([0\,0\,0\,0\,0\,0\,0\,0\,0\,0\,0\,2\,2\,2\,1\,1\,1\,0\,0]) = 6 \end{aligned} \tag{10}$$

Thus this set cannot be a possible result. The set {<*hbfc*, *wpfc*>, <*hbfc*, *ash*>, <*hbfc*, *bw*>} is considered as another example as in

$$\begin{aligned} &\mathbf{sv} = [0\,0\,0\,0\,0\,0\,0\,0\,0\,0\,0\,0\,0\,1\,1\,1\,0\,0] \\ &NUM(\mathbf{sv}) = 3 = NUM(\mathbf{sv} \cdot \mathbf{M}) = \\ &NUM([0\,0\,0\,0\,0\,0\,0\,0\,0\,0\,0\,0\,0\,3\,3\,3\,0\,0]) = 3 \end{aligned} \tag{11}$$

Thus this set is accepted as a possible result. After the test of all the sets of suspected arcs, only two were left as possible results: {<*hbfc*, *wpfc*>, <*hbfc*, *ash*>, <*hbfc*, *bw*>} and {<*hbfc*, *wpfc*>, <*hbfc*, *ash*>, <*hbfc*, *bw*>, <*totalflow*, *bw*>}. The number of possible results decreased from 21 to 2.

The fault diagnosis results, i.e. the two sets of suspected arcs, provide valuable information in identifying the faulty process component in the case of a process fault. The first arc in the first set is <*hbfc*, *wpfc*> corresponding to the process components: a wire section and the white water tray. Similarly, the arcs <*hbfc*, *ash*> and <*hbfc*, *bw*> correspond to the wire section, the wet press and the dryers. Thus the suspected process component is the wire section, since it is located on all three arcs. The same result is obtained from the second set. Moreover, the results also indicated that the fault occurred for the filler material but not for the fiber material.

5. CONCLUSION

A novel dynamic causal digraph reasoning method with the feature of locating process fault on the arcs in the causal digraph was presented in this paper and tested on the short circulation process of the paper machine.

The test results validate that the proposed method is able to provide more information for the fault diagnosis. The improvements offered by the new method are highlighted as a summary of comparison of results in Table 4.

Table 4. Comparison of results between the proposed method and the conventional method

Faults	Fault Type	Dynamic causal digraph		Novel dynamic causal digraph	
		Fault detection	Fault isolation	Fault detection	Fault isolation
Fault 1	Sensor fault	**Nodes**: *defic*	**Fault origin**: *defic*	**Nodes**: *defic*	Fault origin: *defic*
Fault 2	Process fault	**Nodes**: *defc*, *hbfc*, *wpfc*, *ash, bw*	**Fault origins**: *wpfic*, *ash*	**Nodes**: *defc*, *hbfc*, *wpfc*, *ash*, *bw*	**Faulty arcs sets**: {<*hbfc*, *wpfc*>, <*hbfc*, *ash*>, <*hbfc*, *bw*>}, <*hbfc*, *wpfc*>, <*hbfc*, *ash*>, <*hbfc*, *bw*>, <*totalflow*, *bw*>} **faulty component**: Wire section

ACKNOWLEDGEMENTS

This work is financially supported by the Finnish Technology development agency (TEKES). Authors are also very grateful to VTT for providing APROS model as the testing platform.

REFERENCES

Fagarasan, I., S. Ploix and S. Gentil (2004) Causal fault detection and isolation based on a set-membership approach, Automatica, **40,** pp. 2099-2110.

Mogens B., K., Michel, J. Lunze, S., Marcel, *Diagnosis and Fault-Tolerant Control*, Springer-Verlag, Heidelberg, 2003.

Iri, M., K., Aoki, E., O'Shima and H., Matsuyama (1979). An algorithm for diagnosis of system failures in the chemical process, Computer & Chemical Engineering, **3 (1-4)**, pp.489-493

Lappalainen, J., T. Myller, O. Vehviläinen, S. Tuuri and K., Juslin (2003) Enhancing grade changes using dynamic simulation, TAPPI Journal, **2 (12)**.

Leyval, L., S. Gentil and S., Feray-beaumont (1994). Model-based Causal Reasoning for Process Supervision, Automatica, **30**, pp. 1295-1306

Montmain, J. and S., Gentil (2000). Dynamic causal model diagnostic reasoning for online technical process supervision, Automatica, **36**, pp. 1137-1152

Shih R. and L. Lee (1995). Use of Fuzzy Cause-Effect Digraph for Resolution Fault Diagnosis for Process Plants. 1&2. Fuzzy Cause-Effect Digraph, Industrial & Engineering Chemistry Research, **34**, pp. 1688-1717.